Supplementary Materials for

An integrated design for high-energy, durable zinc-iodine batteries with ultra-high recycling efficiency

Leiqian Zhang,[a,‡] Han Ding,[b,‡] Haiqi Gao,[b] Jiaming Gong,[c] Hele Guo,[d] Shuoqing Zhang,[e] Yi Yu,[f] Guanjie He,[g] Tao Deng,[h] Ivan P. Parkin,[g] Johan Hofkens,[d,i] Xiulin Fan,[e,*] Feili Lai,[c,d,*] Tianxi Liu[a,*]

[a] Key Laboratory of Synthetic and Biological Colloids, Ministry of Education, School of Chemical and Material Engineering, Jiangnan University, Wuxi, 214122, P. R. China.

[b] State Key Laboratory of Chemistry and Utilization of Carbon Based Energy Resources, Xinjiang University, Urumqi, 830017, Xinjiang, P. R. China.

[c] State Key Laboratory of Metal Matrix Composites, School of Materials Science and Engineering, Shanghai Jiao Tong University, Shanghai, 200240, P. R. China.

[d] Department of Chemistry, KU Leuven, Celestijnenlaan 200F, Leuven 3001, Belgium.

[e] State Key Laboratory of Silicon and Advanced Semiconductor Materials, School of Materials Science and Engineering, Zhejiang University, Hangzhou, 310027, P. R. China.

[f] School of Chemical Engineering, Zhengzhou University, Zhengzhou, 450001, P. R. China.

[g] Department of Chemistry, University College London, London, WC1H 0AJ, UK.

[h] China-UK Low Carbon College, Shanghai Jiao Tong University, Shanghai, 201306, P. R. China.

[i] Department of Molecular Spectroscopy, Max Planck Institute for Polymer Research, Ackermannweg 10, Mainz 55128, Germany.

*Corresponding author: Email: xlfan@zju.edu.cn (X. Fan); feililai@sjtu.edu.cn (F. Lai); feili.lai@kuleuven.be (F. Lai); txliu@jiangnan.edu.cn (T. Liu)

‡These authors contributed equally to this work.

Experimental procedures

Materials

Anhydrous magnesium sulfate ($MgSO_4$, ≥98%), tetrabutylammonium iodide (TBAI, ≥99%), acetonitrile (AN, 99.9%), 1-butyl-3-methylimidazolium hexafluorophosphate ([BMIM]PF_6, ≥99%), iodine (99%), sodium chloride (NaCl, 99.999%), and zinc sulfate heptahydrate ($ZnSO_4$, ≥99.5%) were purchased from Shanghai Titan Technology Co. Ltd. Carbon felt was adopted from Tianjin Aosen Carbon Co. Ltd. All chemicals were used as received.

Battery assembly

The configuration of the self-sieving polyiodide-capable liquid-liquid biphasic system (1T-7A3B/2Z0.5M-W) was illustrated in **Fig. 3a**. The organic electrolyte was composed of AN containing 1 M TBAI and [BMIM]PF_6 in a ratio of 7:3 (v/v). The aqueous electrolyte comprised 2 M $ZnSO_4$ and 0.5 M $MgSO_4$ in deionized water. The volume ratio of the organic to aqueous phase was 1:5. To enhance the energy density of batteries, additional solid iodine (0.5, 0.75, and 1.0 M) could be introduced into the organic phase. Besides, the realization of the two-electron iodine conversion reaction (I^-/I^+) within the 1T-7A3B/2Z0.5M-W system was achieved through the addition of 1 M NaCl to the aqueous phase. A standardized 1 mL of organic electrolyte was utilized in all routine tests. The positive current collector featured a carbon felt electrode measuring 2 cm (length) × 2 cm (width) × 0.8 cm (height), while the anode consisted of a zinc foil with a diameter of 1.6 cm and a thickness of 0.1 mm. Copper and titanium were employed as negative and positive wires, respectively. Subsequently, the battery was sealed using the hot melt adhesive to avoid electrolyte volatilization. A similar assembly procedure was followed for larger-scale batteries. Zinc-bromine battery was assembled following the design of the 1T-7A3B/2Z0.5M-W system, with TBAI replaced by tetrabutylammonium bromide (0.5 M).

Battery tests

The galvanostatic charge/discharge characterization of the cells was conducted using a LAND-CT2003A system within a voltage window of 0.6−1.6 V (*vs.* Zn^{2+}/Zn) at varying rates ranging from 0.1−2 C (with 1 C corresponding to 211 mA g^{-1}_{iodine}) at 25 ℃. The specific capacity of batteries was determined based on the iodine content in the electrolyte. Cyclic voltammetry (CV) measurements were performed on a CHI660E electrochemical workstation at a scan rate of 0.1 mV s^{-1}. Electrochemical impedance spectroscopy was conducted using a CHI660E electrochemical workstation, employing an AC amplitude of 10 mV and a frequency range spanning 0.1 to 10^5 Hz under open-circuit voltage conditions. The energy storage module comprised four 1T-7A3B/2Z0.5M-W cells connected in series, each containing 10 mL of organic electrolyte (2.2 M I^-). Charging of the energy storage module was facilitated by a 30 W solar panel, with the voltage variations during charging being monitored in real-time. The discharge process was carried out using an electrochemical workstation with a current of 50 mA. Battery self-discharge tests were conducted using a 1T-7A3B/2Z0.5M-W system with 1 mL of organic phase at room temperature. Specifically, the battery was first charged to 1.6 V following four charge/discharge cycles at a current density of 0.5 C, after which it was allowed to rest. At predetermined time intervals, the battery was then discharged at 0.5 C. This process was repeated to systematically evaluate the self-discharge performance of the battery at different resting times (0.5, 1, 2, 4, 8, and 30 d).

Characterization

The ionic conductivity was evaluated using the FE38-Standard at 25 ℃. Volatility assessments were conducted by measuring the weight loss of various component solutions at room temperature under ambient conditions. The oil-water distribution ratio was determined by quantifying the volume variance between two phases after mixing. The interface overpotential was determined by employing the four-electrode method reported in the literature.[1] The partition coefficient (Log *P*) was calculated utilizing the following equation:

$$\text{Log } P = \text{Log} \frac{C_o}{C_w} \quad (1)$$

where C_o and C_w represent the concentrations of polyiodide in the organic and aqueous phases, respectively. C_w can be deduced from the polyiodide concentration determined *via* a standard curve of polyiodide in the aqueous phase (**Fig. S4**).

In situ ultraviolet-visible spectroscopy (UV-vis) and Raman analysis

In situ UV-vis analysis was performed using a TU-1900 spectrophotometer equipped with a customized quartz cell (**Fig. S15a**). The scanning interval during observation was set at three minutes with a current of 0.2 mA. In situ Raman spectroscopy tests were conducted utilizing an inVia InSpect instrument with a customized quartz tube (**Fig. S15b**). The scanning interval was adjusted to five minutes with a current of 0.5 mA.

Ion concentration measurement

The quantifications of Zn^{2+}, Mg^{2+}, and SO_4^{2-} ions in the aqueous phase were conducted using inductively coupled plasma optical emission spectroscopy (ICAP 7400). I^- ions were scrutinized *via* ion chromatography (Dionex Inuvion). $BMIM^+$ ions were identified through UV-vis spectroscopy (TU-1900). During the UV-vis analysis, Ag_2SO_4 was initially utilized to precipitate I^- ions, followed by the addition of NaCl to eliminate any excess Ag^+ ions, thus preventing signal interference between ions. Subsequent centrifugation led to the collection of the upper layer of the clarified solution for the determination of $BMIM^+$ ion concentration. Further analysis of PF_6^- and TBA^+ ions was carried out using nuclear magnetic resonance (NMR, AVANCE NEO 600M) spectroscopy. The samples (0.5 mL) underwent a drying process to remove water before being diluted with D_2O (0.6 mL). ^1H NMR spectra were utilized for TBA^+ ion analysis, with $BMIM^+$ ions serving as an internal calibrant. Additionally, ^{19}F NMR spectra were employed to ascertain the concentration of PF_6^-, with the inclusion of $CF_3SO_3^-$ as the internal calibrant.

Electrolyte recovery experiment

For the electrolyte recovery experiment, a 1T-7A3B/2Z0.5M-W system containing 8 mL of organic electrolyte (2.2 M I^-) was utilized. Initially, the battery underwent aging at 0.2 C before being disassembled. Subsequently, the organic and aqueous phases were separated using a separatory funnel. The graphite felt was then subjected to repeated soaking and washing with AN, while the wash solution was recovered and combined with the organic phase. The iodine-containing organic solution obtained was further concentrated through spin distillation. Finally, the collected aqueous and organic solutions (supplemented with AN to a total volume of 8 mL) were employed to reassemble the cell for subsequent electrochemical performance testing.

Molecular dynamics (MD) simulations

The molecular structures of TBAI (optimized with the B3LYP/LANL2DZ basis set), $[BMIM]PF_6$ (optimized with the B3LYP/DGDZVP basis set), AN (optimized with the B3LYP/6-311G basis set), SO_4^{2-} ions (optimized with the B3LYP/6-311G(d) basis set), and elemental iodine (optimized

with the B3LYP/DGDZVP basis set) were generated using GaussView 6.0, while their structural optimizations were performed using Gaussian 09. MD simulations were conducted using the GROMACS2021.7 software package.[2] The OPLS-AA force-field parameters were applied for TBAI, [BMIM]PF_6, AN, H_2O, SO_4^{2-}, polyiodide, Zn^{2+}, and Mg^{2+}.[3] The total numbers of TBAI, [BMIM]PF_6, AN, SO_4^{2-}, Mg^{2+} Zn^{2+}, H_2O, and I_2 in simulated system were 152, 317, 1455, 1500, 300, 1200, 8888, and 152, respectively.

All simulations were firstly energy minimized at temperature of 298.15 K, and then NPT ensemble was conducted at 298.15 K and 1 bar. Temperature and pressure were regulated using the velocity-rescale thermostat and Berendsen barostat with coupling constants of 1.0 ps.[4,5] Periodic boundary conditions were applied in all three dimensions of the simulation systems, and a leap-frog integration algorithm with a time step of 1 fs was employed. Each MD simulation was run for 100 ns to ensure equilibration.

The cumulative distribution function (CDF, *n(r)*) between particles of type A (ions/molecules) and B (water/AN) can be calculated through the radial distribution function (RDF, *g(r)*) using the following equation:

$$n_{AB}(r) = \int_0^r 4\pi r^2 \rho_B g_{AB}(r)\,\mathrm{d}r \tag{2}$$

Where ρ_B represents the average number density of water/AN molecules in the bulk phase, and *r* denotes the distance between ions/molecules and water/AN.

Density functional theory (DFT) calculations

All calculations were performed in the Accelrys Material Studio DMol3 module. I_3^- and TBA^+, $[BMIM]^+$, AN, and H_2O were optimized by generalized gradient approximation (GGA) and Perdew-Burke-Ernzerh (PBE) functional form.[6] The valence orbitals of atoms were described using double numerical plus polarization (DNP) basis sets.[7] The convergence criterion for the self-consistent field calculations was $1e^{-6}$ Hartree, while the tolerances of energy, maximum force, and maximum displacement for geometry optimization were 0.00001, 0.002, and 0.005 au, respectively. To better explore the potential energy surface, several initial configurations were established for the structure optimization. The binding energy (E_b) between A (I_3^-) and B (TBA^+, $[BMIM]^+$, AN, and H_2O) was defined as the following equation (3):

$$E_b = E_{A-B} - E_A - E_B \tag{3}$$

where $E_{A\text{-}B}$, E_A, and E_B represent the total energies of A (I_3^-) with B (TBA^+, $[BMIM]^+$, AN, and H_2O), A (I_3^-), and B (TBA^+, $[BMIM]^+$, AN, and H_2O), respectively.

Supporting figures

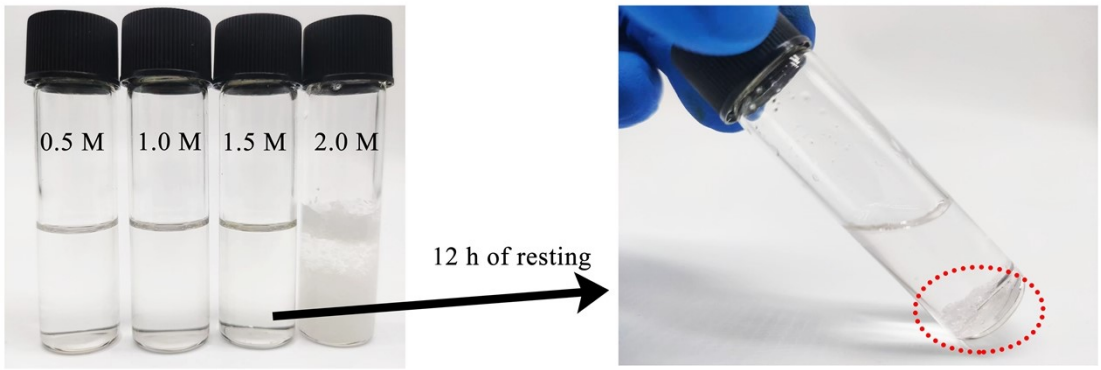

Fig. S1 Images of AN containing varying concentrations of TBAI. While AN is capable of dissolving 1.5 M of TBAI through sonication, precipitation of TBAI occurs following 12 h of standing time.

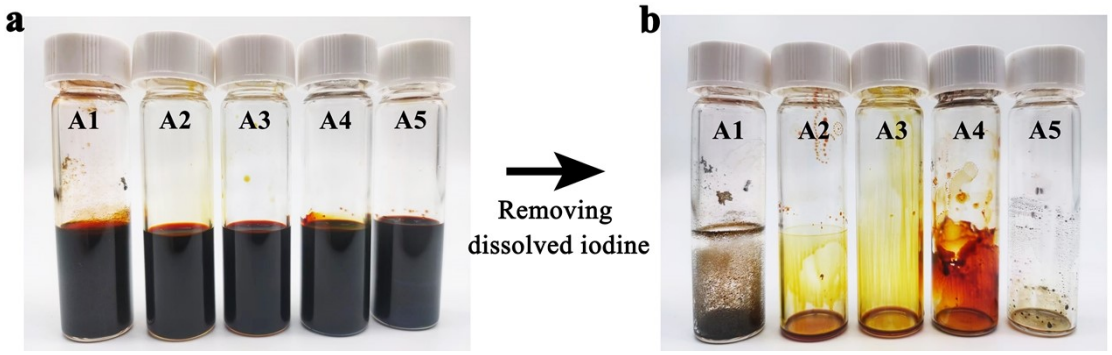

Fig. S2 a) Images of AN or 1T-AN solutions with varying iodine concentrations. A1 depicts AN with 0.5 M I_2, while A2, A3, A4, and A5 correspond to 1T-AN solutions containing 0.5, 1.0, 1.5, and 2.0 M I_2, respectively. b) The corresponding digital images after removing dissolved iodine. A substantial amount of insoluble iodine was observed in AN with 0.5 M I_2, whereas minimal solid iodine was present in 1T-AN even at a concentration of 2 M I_2.

Fig. S3 Images of a) the polyiodide solution, and b) the polyiodide solution with TBAI. Upon the addition of TBAI to the polyiodide solution, the color of the polyiodide solution transitioned from brownish-red to colorless, indicating the robust adsorption of TBAI on polyiodide ions.

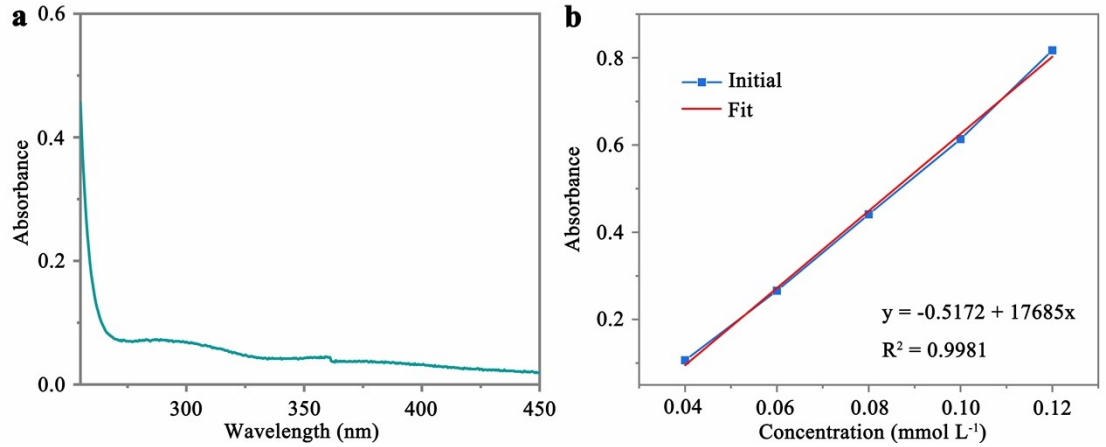

Fig. S4 a) UV-vis spectrum of the aqueous phase in the 1T-7A3B/2Z0.5M-W system containing 0.2 M I_2. b) Standard curve illustrating the correlation between the concentration of I_3^- and absorbance.

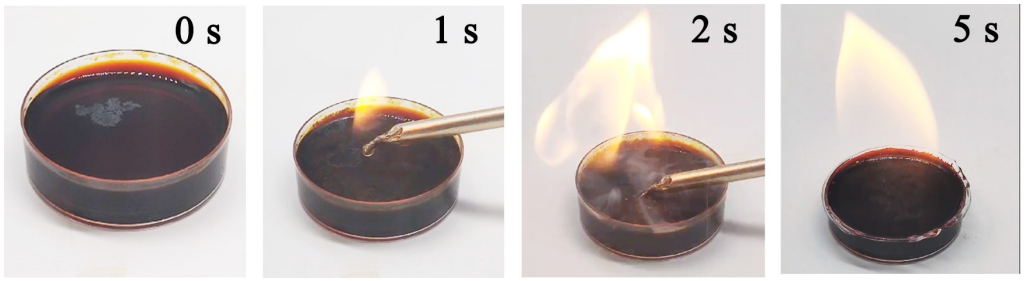

Fig. S5 Flammability assessment of AN/2Z0.5M-W (i.e., 1T-7A3B/2Z0.5M-W system without TBAI and [BMIM]PF_6).

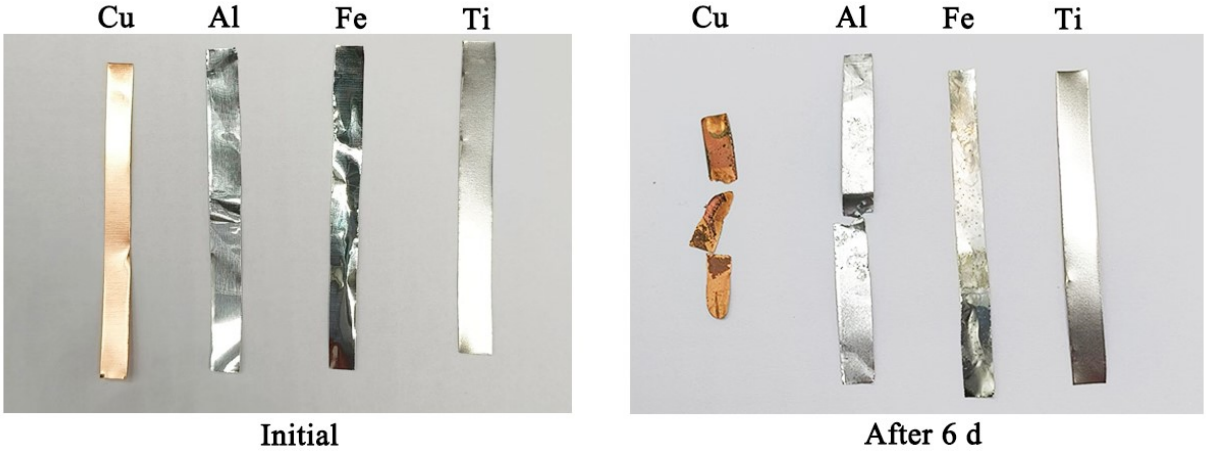

Fig. S6 Comparison of Cu, Al, Fe and Ti before and after corrosion of the organic phase containing 2.2 M iodide ions at 40 °C for 6 days.

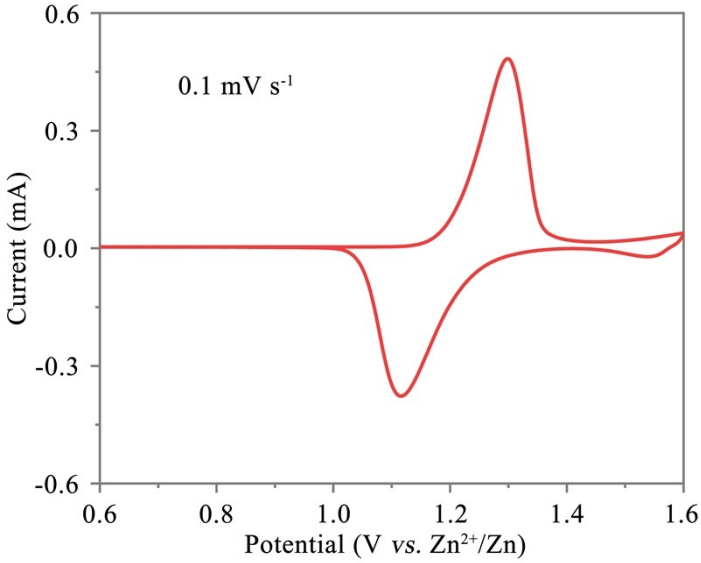

Fig. S7 CV curve of 1T-7A3B/2Z0.5M-W system at a scan rate of 0.1 mV s^{-1}.

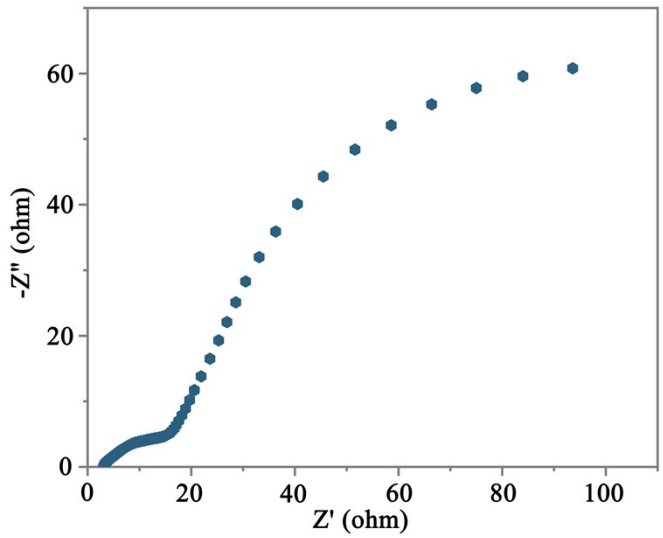

Fig. S8 Electrochemical impedance spectroscopy of the 1T-7A3B/2Z0.5M-W system.

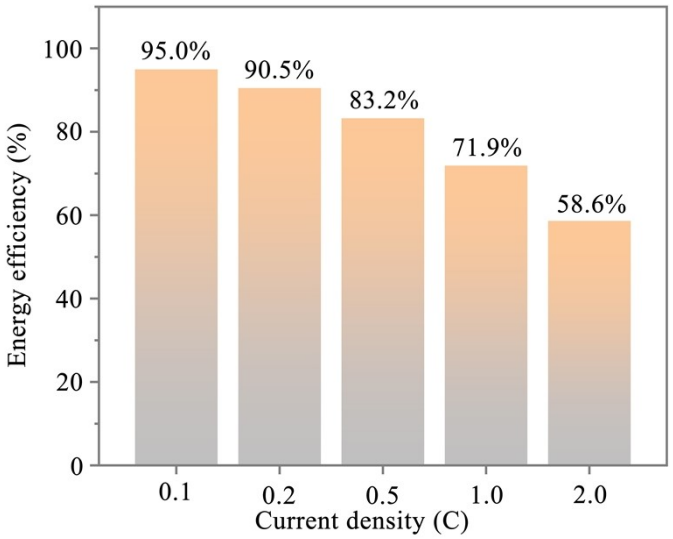

Fig. S9 Energy efficiency of 1T-7A3B/2Z0.5M-W system at various current densities.

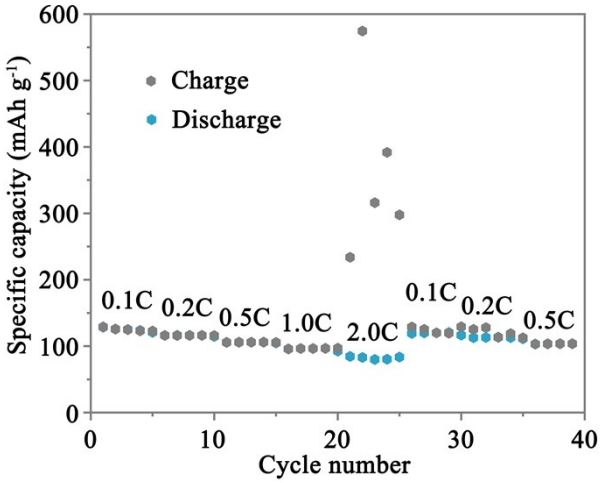

Fig. S10 Rate performance of 1T-7A3B/2Z0.5M-W system with TBAI replaced by equimolar solid iodine (0.35 M).

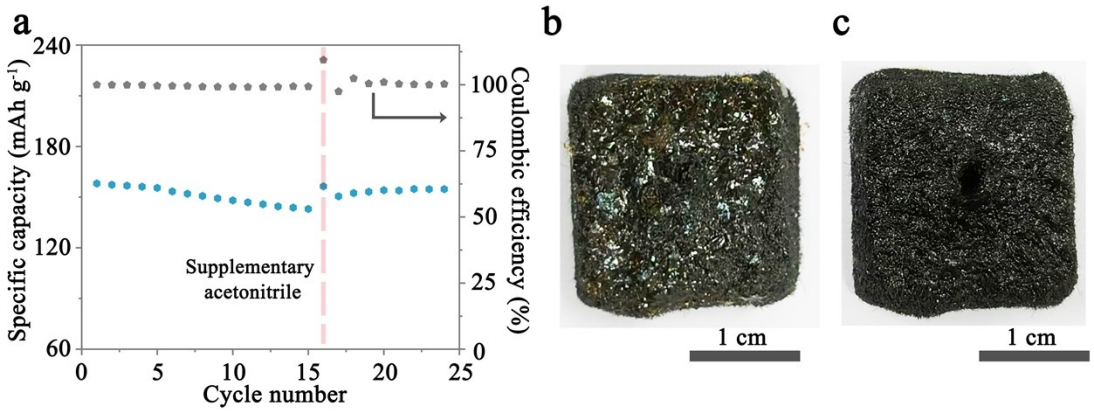

Fig. S11 a) Cycling performance of an unencapsulated cell model with the organic phase exposed to an open environment at 0.5 C. Digital images of the electrodes obtained b) before and c) after the introduction of AN following 15 cycles in a parallel set of experiments. In the open-structured biphasic battery system, the volatilization of AN was found to promote the precipitation of salts within the electrodes, leading to a reduction in battery capacity. Notably, the lost capacity can be recovered through the re-dissolution of the salts by reintroducing AN.

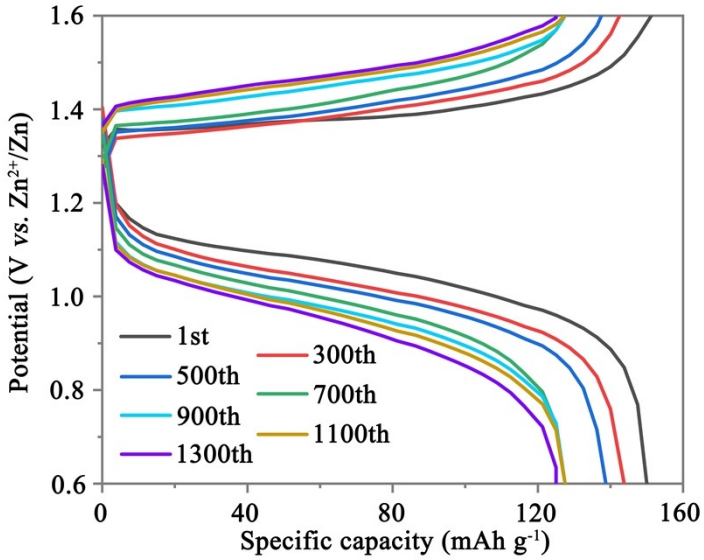

Fig. S12 a) Charge-discharge curves of 1T-7A3B/2Z0.5M-W system after different cycles at 1 C.

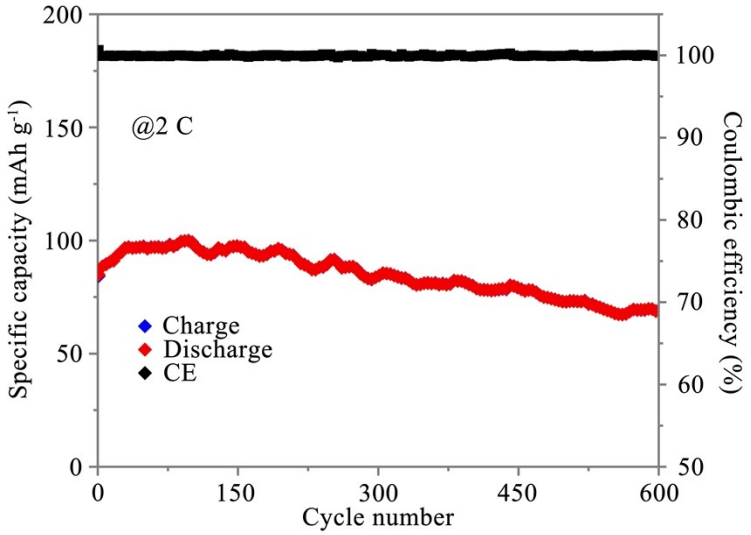

Fig. S13 Cycling performance of 1T-7A3B/2Z0.5M-W system at 2 C.

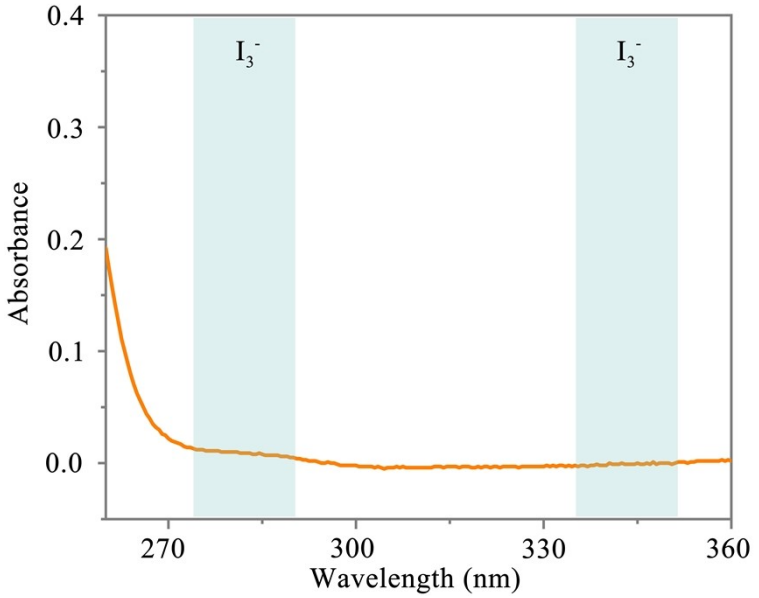

Fig. S14 UV-vis spectrum of the aqueous phase obtained from 1T-7A3B/2Z0.5M-W system after 600 cycles at 2 C.

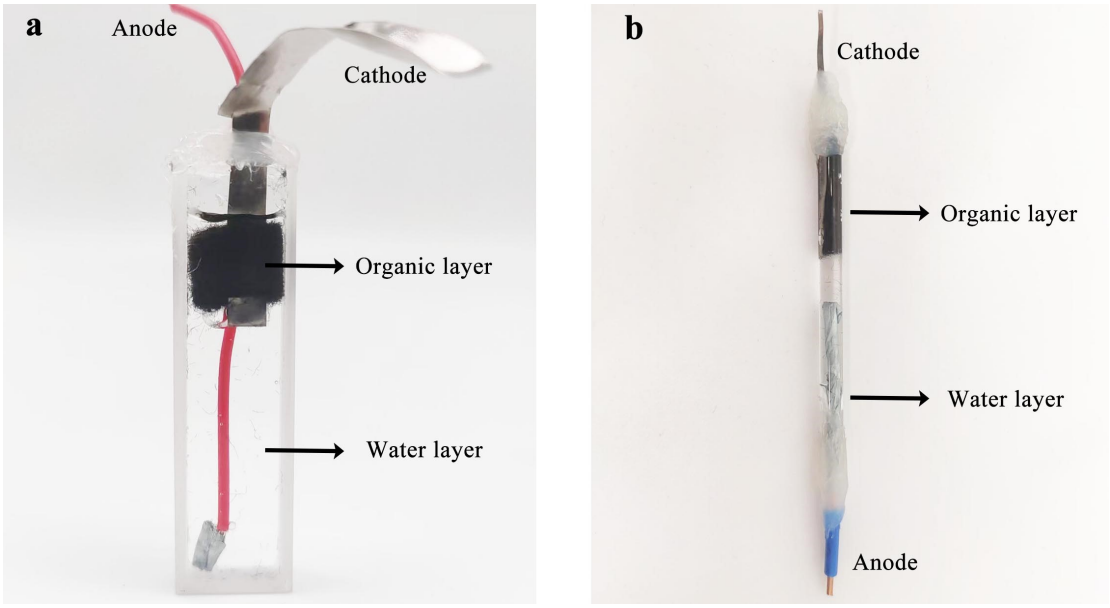

Fig. S15 Images of a) in situ UV-vis, and b) in situ Raman experimental configurations.

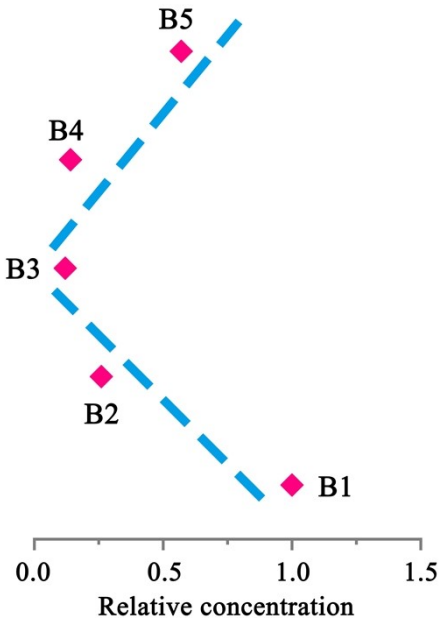

Fig. S16 Changes in the relative concentration of zinc ions, in the organic layer at different SOCs (B1: open-circuit voltage; B2: 1.3 V; B3: 1.6 V; B4: 1.1 V; B5: 0.6 V).

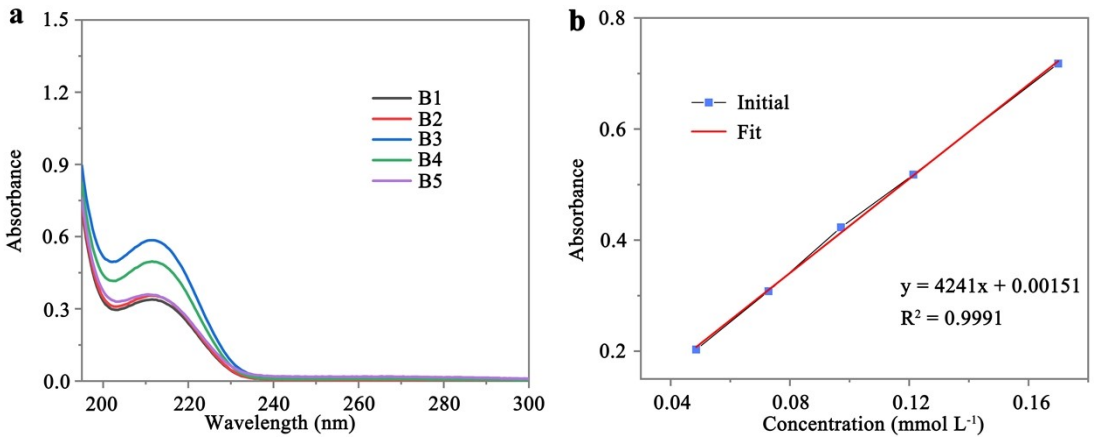

Fig. S17 a) UV-vis spectra of $BMIM^+$ ions in the aqueous phase at various SOCs (B1: open-circuit voltage; B2: 1.3 V; B3: 1.6 V; B4: 1.1 V; B5: 0.6 V). b) Standard curve revealing relationship between concentration of $BMIM^+$ and absorbance.

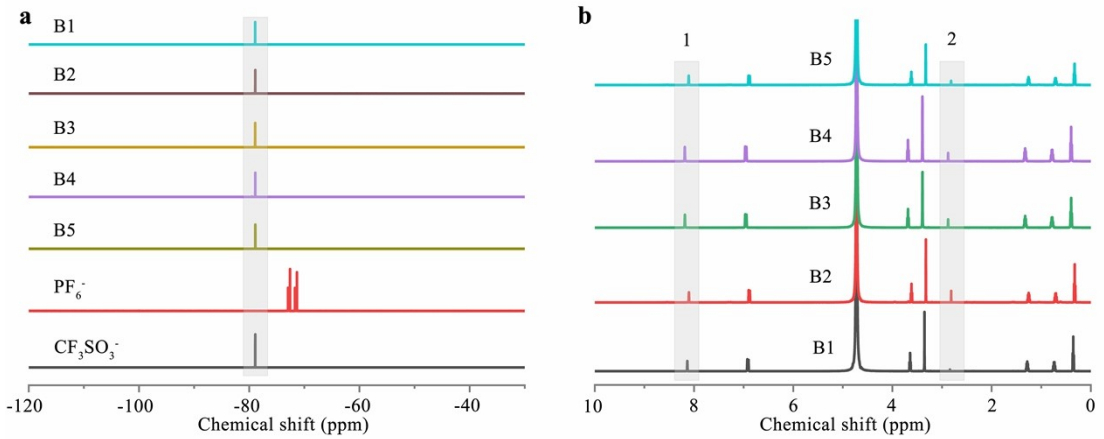

Fig. S18 a) ^{19}F NMR spectra of the aqueous phase at various SOCs (B1: open-circuit voltage; B2: 1.3 V; B3: 1.6 V; B4: 1.1 V; B5: 0.6 V) using $CF_3SO_3^-$ ions as an internal standard. No signal corresponding to PF_6^- is detected, indicating the absence of PF_6^- in the aqueous phase. b) ^1H NMR spectra of the aqueous phase at different SOCs. By utilizing the known concentration of $BMIM^+$ as the internal standard, the concentration of TBA^+ can be calculated based on the ratio of characteristic peak areas of $BMIM^+$ (1) and TBA^+ (2). The $BMIM^+$ to TBA^+ ratios in B1, B2, B3, B4, and B5 are 15.20:1, 2.85:1, 2.42:1, 2.86:1, and 3.84:1, respectively.

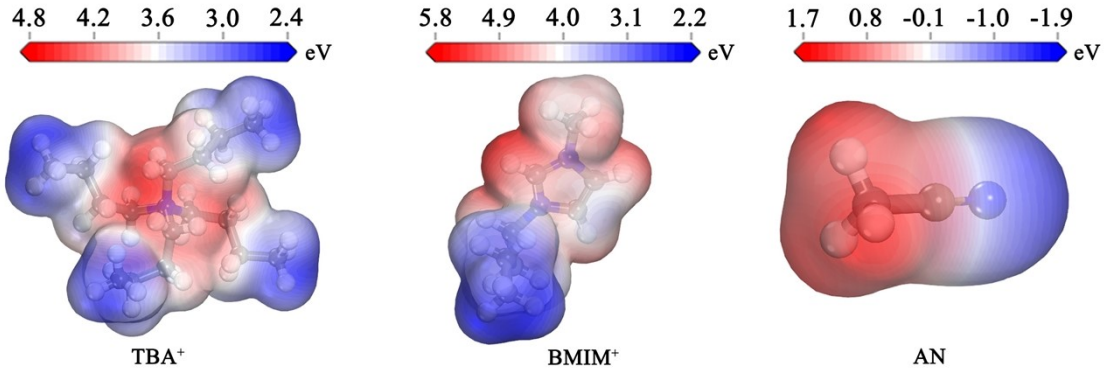

Fig. S19 Electrostatic potential distributions of TBA^+, $BMIM^+$, and AN.

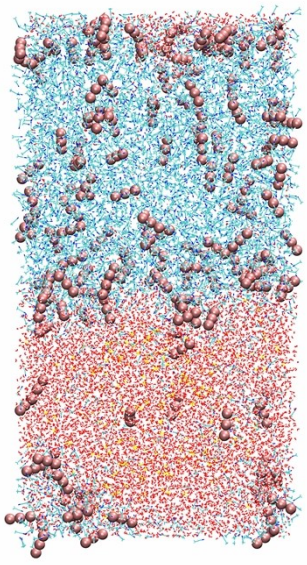

Fig. S20 Polyiodide distribution in the 1T-7A3B/2Z0.5M-W system in the absence of TBAI and [BMIM]PF_6 at 5 ns.

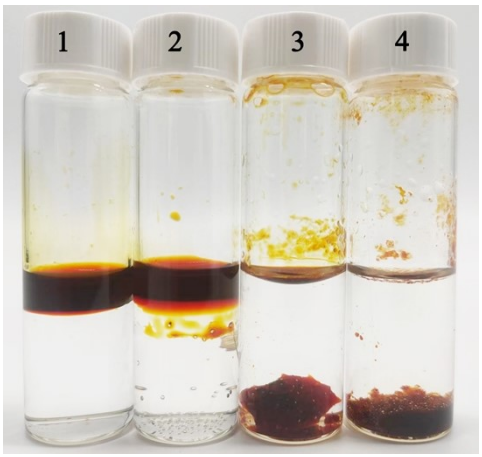

Fig. S21 1T-7A3B/2Z0.5M-W systems with varying salt concentrations in the aqueous phase: (1) 2 M $ZnSO_4$ + 0.5 M $MgSO_4$; (2) 2 M $ZnSO_4$; (3) 1 M $ZnSO_4$; (4) 0 M $ZnSO_4$.

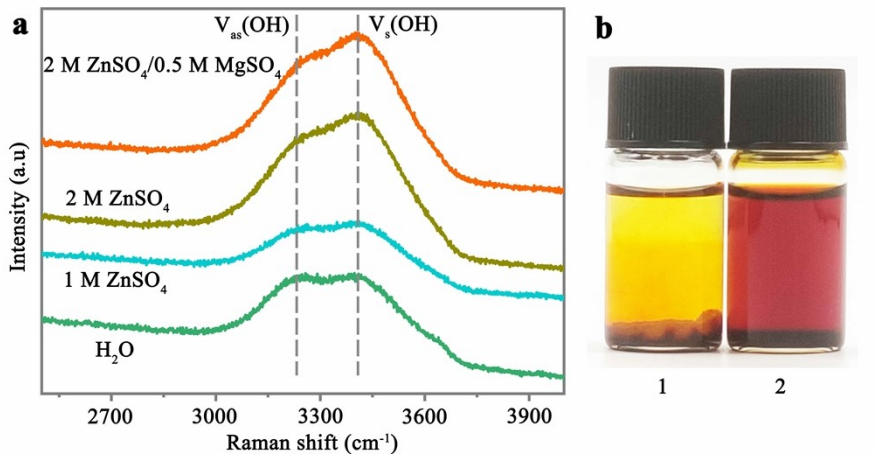

Fig. S22 a) Raman spectra of aqueous solutions with varying salt concentrations. With increasing salt concentration, the V_{as}(OH) peak of the −OH group in H_2O (~3227 cm^{-1}) diminishes, while the area of its V_s(OH) peak (~3400 cm^{-1}) expands, indicating a reduction in free water content.[8] b) Digital images of polyiodide in 2 M $ZnSO_4$/0.5 M $MgSO_4$ (1) and pure water (2). Evidently, due to the decreased presence of free water molecules, the solubility of polyiodide in 2 M $ZnSO_4$/0.5 M $MgSO_4$ is significantly lower than that in pure water.

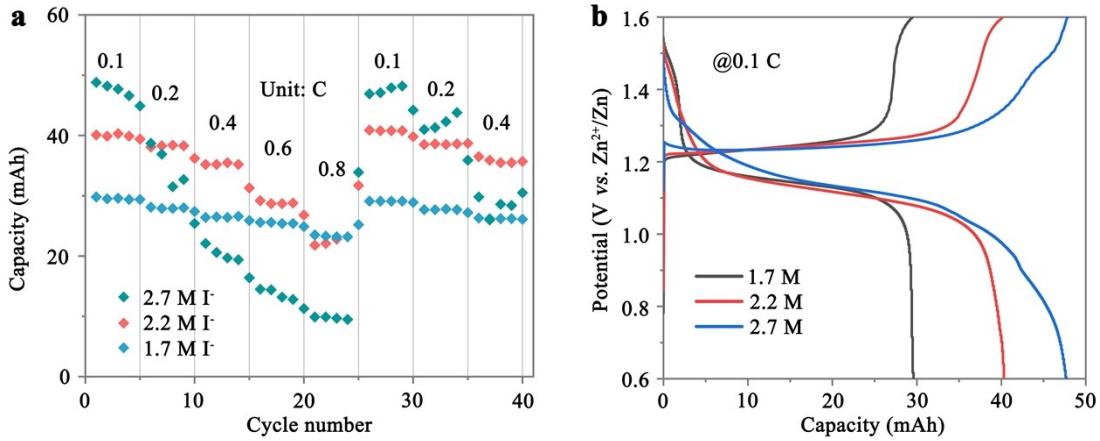

Fig. S23 a) Rate performance of 1T-7A3B/2Z0.5M-W system with different concentrations of iodide ions at various current densities. b) Charge-discharge profiles of the 1T-7A3B/2Z0.5M-W system with 1.7, 2.2, and 2.7 M I^- at 0.1 C.

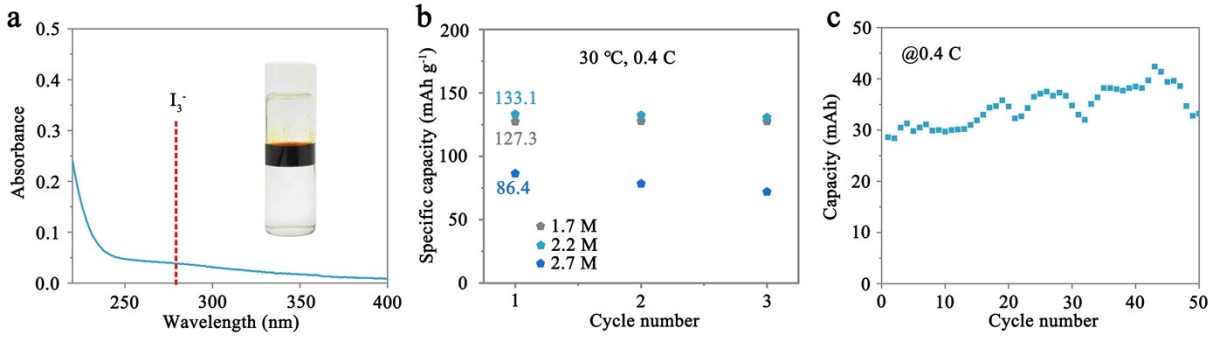

Fig. 24 a) UV-vis spectrum of the aqueous phase within a biphasic system containing 2.7 M iodide ions in the organic phase (top). The inset displays a digital image of the corresponding biphasic system, which reflects that the instability of the 2.7-ZIB cannot be attributed to the occurrence of polyiodide shuttling. b) Evaluation of specific capacity for batteries with varying iodide ion concentrations at 30 °C under a current density of 0.4 C. Considering that the specific capacities of the biphasic systems with 1.7, 2.2, and 2.7 M iodide ions at 25 °C were measured as 122.4, 126.1, and 64.5 mAh g^{-1}, respectively; these results underscore the pronounced sensitivity of the specific capacity in batteries containing 2.7 M iodide ions to temperature variations. c) Cycling performance of the 1T-7A3B/2Z0.5M-W system with 2.7 M I^- at 0.4 C.

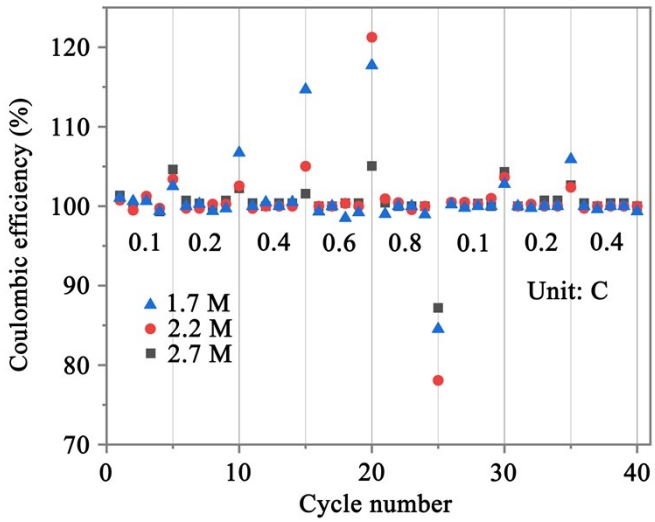

Fig. S25 CE of 1T-7A3B/2Z0.5M-W system with different concentrations of iodide ions at various current densities.

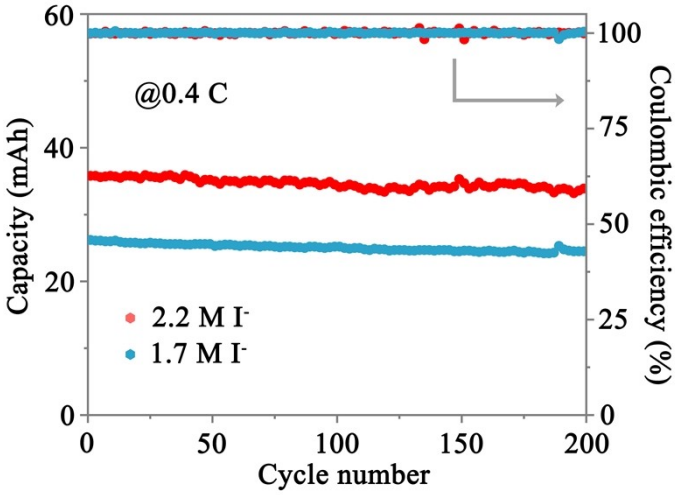

Fig. S26 Cycling performance assessment of the 1T-7A3B/2Z0.5M-W system with 1.7 and 2.2 M I^- at 0.4 C.

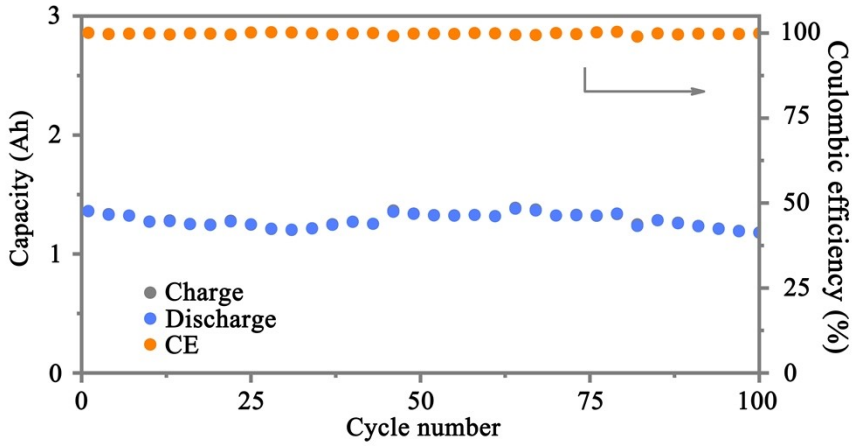

Fig. S27 Evaluation of cycling performance of the Ah-level 1T-7A3B/2Z0.5M-W system at a current of 100 mA.

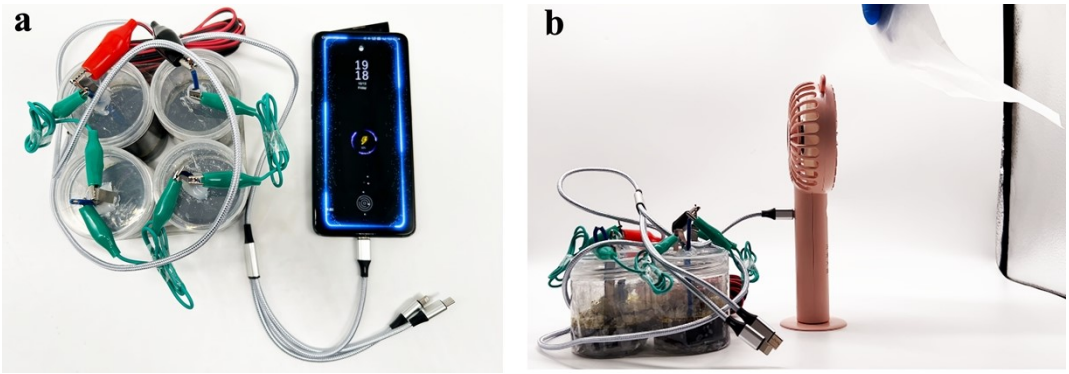

Fig. S28 Powering a) a cell phone, and b) an electric fan with the 1T-7A3B/2Z0.5M-W system.

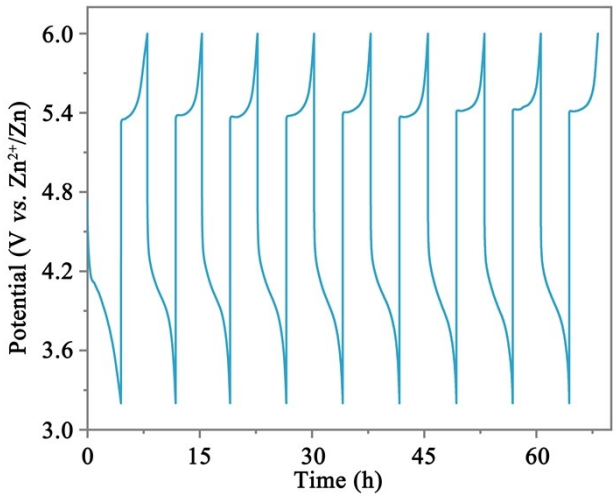

Fig. S29 Cycling stability of a four-series-connected 1T-7A3B/2Z0.5M-W system at 0.15 C.

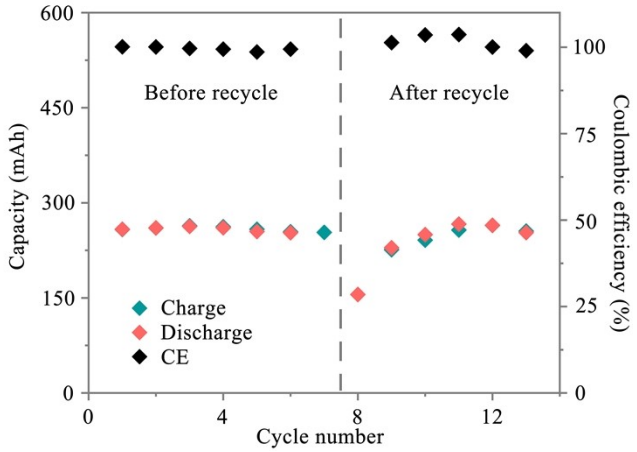

Fig. S30 Cycling performance of 1T-7A3B/2Z0.5M-W system before and after reusing the electrolyte.

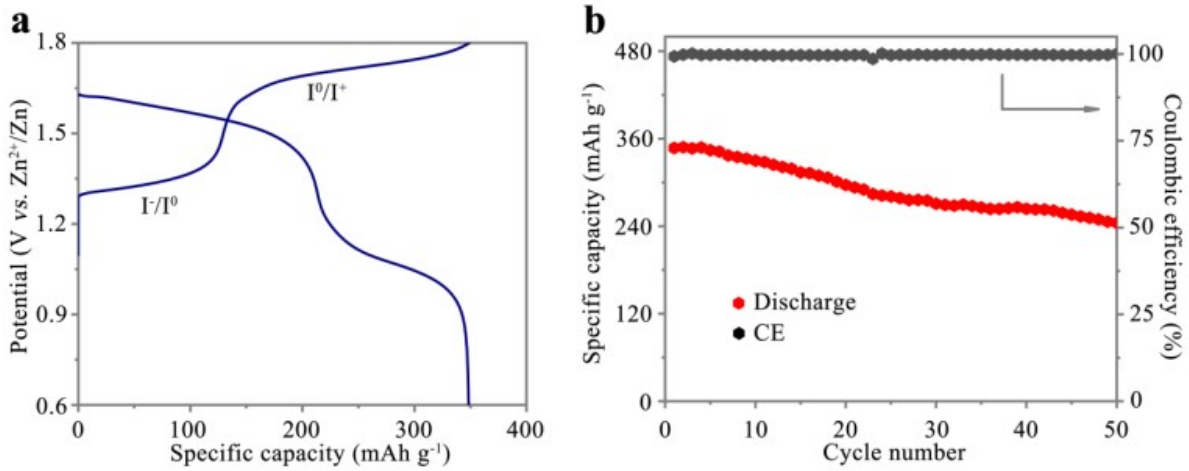

Fig. S31 a) Charge/discharge curves for the 1T-7A3B/2Z0.5M-W system capable of two-electron reaction processes (I^{-}/I^{+}) at 0.5 C. In comparison to the one-electron process, the two-electron iodine conversion process not only significantly enhances the specific capacity of the 1T-7A3B/2Z0.5M-W system (348.4 mAh g^{-1}) but also elevates the discharge voltage (median discharge voltage: 1.49 V), resulting in an impressive energy density of up to 474.1 Wh kg^{-1} (based on the iodine mass). This will effectively enhance the competitiveness of the 1T-7A3B/2Z0.5M-W system for large-scale energy storage. b) Cycling performance of the 1T-7A3B/2Z0.5M-W system based on the two-electron iodine conversion processes at 0.5 C.

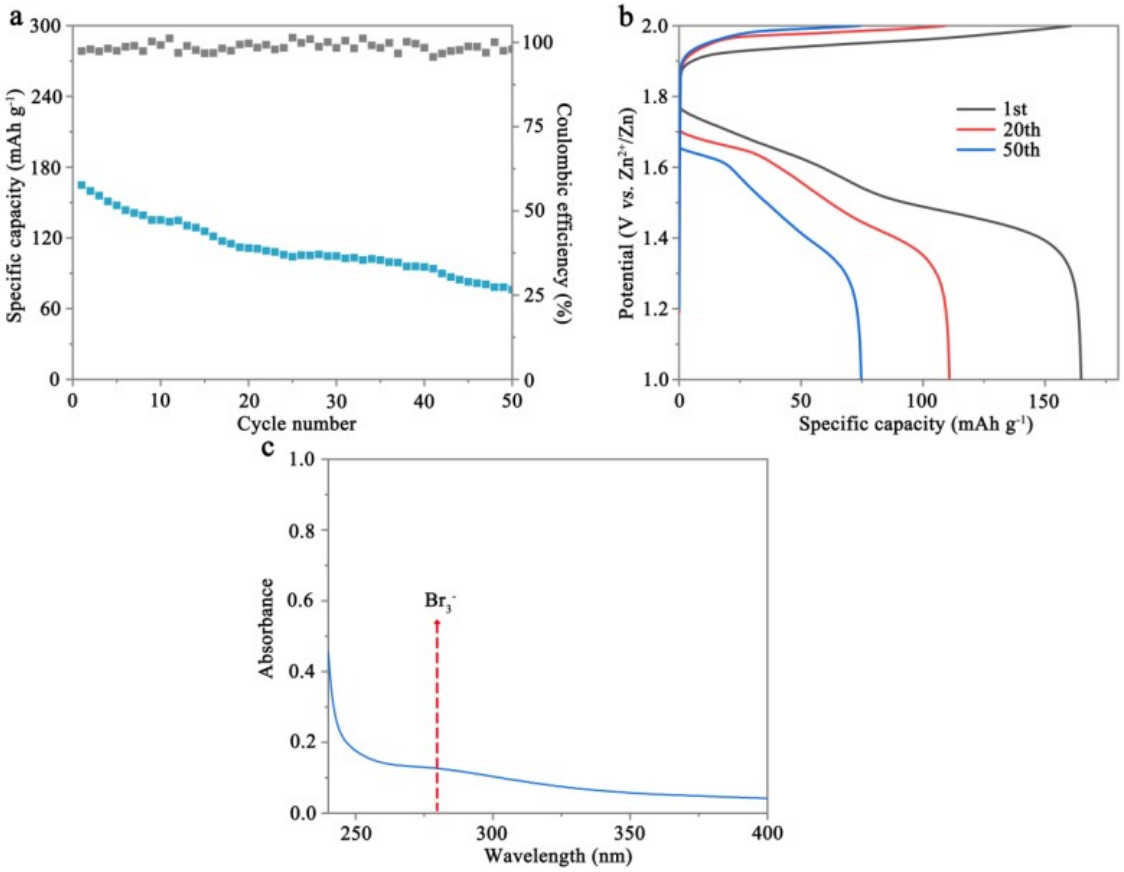

Fig. S32 a) Cycling stability of a zinc-bromine battery constructed based on the 1T-7A3B/2Z0.5M-W system at 1 C, and b) the corresponding charge/discharge voltage profiles at various cycles. c) UV-vis spectrum of the aqueous phase after 50 cycles. The low concentration of polybromide in the aqueous phase underscores the effective mitigation of polybromide shuttling in the battery.

Table S1. Key electrochemical parameters of zinc-iodine batteries for statistical year 2023-2024, highlighting iodine loading, self-discharge rate, and renewability (iodine host materials in black; alternative strategies, including modified membranes/interlayers/electrolytes, in blue).

Year	Iodine loading (mg cm^{-2})	CE (%) after resting (h)	Calculated self-discharge rate (%, per day)	Recyclability	Ref.
2023	1.0–1.2				9
2023	2				10
2023	2.5				11
2023	2.5	99.2 (72)	0.3		12
2023	3	91 (12)	18.0		13
2023	0.5-1				14
2023	2				15
2023	0.8-1.5	81 (70)	6.5		16
2023	3.5–4.5				17
2023	0.8-1.2	83.3 (24)	16.7		18
2023	1-1.2				19
2024	18	65.8 (144)	5.7		20
2024	1.0-1.2				21
2024	2	78 (125)	4.2		22
2024	2.0-2.5				23
2024		93 (24)	7		24
2024	~16.3				25
2024	3				26
2024	1-2	98.8 (24)	1.2	Recyclable binder	27
2024	0.8-1.2				28
2024	7.82				29
2024	2				30
2024	0.8-1.2				31
2024	2				32
2024	3				33
2024	14.1	88.2 (48)	5.9		34
2024	0.8–1.2	1.7%/h	40.8		35
2024	1	85 (12)	30		36
2023	3.15				37
2023	1.8–2.0				38
2023	0.8-1.8				39
2023	1.2				40
2023	5	82.3 (20)	21.2		41
2023	1.5				42
2023	25.33				43
2023	2.5-2.8	90.5 (48)	4.8		44
2023	2	65 (48)	17.5	Recyclable membrane	45
2023	8	96.7 (48)	1.65		46

2023	1	99.8 (24)	0.2		47
2023	2-3	90.44 (48)	4.8		48
2023		96 (48)	2		49
2023	33.3				50
2023	20				51
2024		86.8 (24)	13.2		52
2024	5.2				53
2024		78 (24)	22		54
2024	2.4				55
2024	0.8-1.5				56
2024	3	97.5 (5)	12		57
2024	38				58
2024	0.8-1.5				59
2024	0.6	85 (72)	5.0		60
2024	1	85.9 (12)	28.2		61
2024					62
2024	35	88.3 (30 day)	0.4		63
2024	~9.5	93.1 (48)	3.5		64
2024		96.8 (20)	3.8		65
2024		90.42 (48)	4.8		66
2024	1-1.3				67
2024	10				68
2024		94.9 (48)	2.6		69
2024	2-3	90.3 (48)	4.9		70
2024	0.8-1.0	90.2 (48)	4.9		71
2024	37.5				72
2024	35	95.53 (48)	2.2		73
2024	9	90.89 (48)	4.6		74
2024	1.5–2.0	82.9 (41 day)	0.4		75
2024	1	87.8 (48)	6.1		76
2024	69.8	96.6 (30 day)	0.1	~100 % recovery efficiency of active substances	This work

Table S2. Material cost analysis for 1 liter of electrolyte in the 1T-7A3B/2Z0.5M-W system based on the organic phase containing 2.2 M of iodide ions (1 mL, 40.1 mAh).

Raw material	Unit weight price* ($ kg^{-1})	Weight (g)	Cost ($)
$ZnSO_4$	2.1	479.3	1.0
$MgSO_4$	0.1	50.0	0.005
TBAI	3.5	43.1	0.2
$[BMIM]PF_6$	44.6	69.0	3.0
Iodine	8.0	31.7	0.3
AN	1.3	57.0	0.1
Total cost			4.6

Table S3. Content analysis of the components within 1T-7A3B/2Z0.5M-W system based on the organic phase containing 2.2 M of iodide ions. The high proportion of the aqueous phase results in a diminished iodine content; thus, reducing the water-to-organic phase ratio represents an effective strategy for enhancing the energy density of the 1T-7A3B/2Z0.5M-W system.

	AN	Water	TBAI	Iodine	$ZnSO_4$	$MgSO_4$	$[BMIM]PF_6$
Mass content (wt%)	4.4	43.8	3.3	2.4	36.9	3.9	5.3
Volume content (vol%)	7.3	56.9	3.6	0.8	24.5	1.9	5.0

References

1. I. Hatay, B. Su, F. Li, M. A. Me´ndez, T. Khoury, C. P. Gros, J.-M. Barbe, M. Ersoz, Z. Samec, H. H. Girault, *J. Am. Chem. Soc.* **131**, 13453–13459 (2009).
2. M. J. Abraham, T. Murtola, R. Schulz, S. Páll, J. C. Smith, B. Hess, E. Lindahl, *SoftwareX*, **1-2**, 19-25 (2015).
3. W. L. Jorgensen, D. S. Maxwell, J. Tirado-Rives, *J. Am. Chem. Soc.* **118**, 11225-11236 (1996).
4. X. Zhang, Y. Wang, J. Mi, J. Jin, H. Meng, *Chem. Eng. J.* **451**, 139000 (2023).
5. H. J. C. Berendsen, J. P. M. Postma, W. F. van Gunsteren, A. DiNola, J. R. Haak, *J. Chem. Phys.* **81**, 3684-3690 (1984).
6. J. P. Perdew, K. Burke, M. G. Ernzerhof, *Phys. Rev. Lett.* **77**, 3865 (1996).
7. B. Delley, *J. Chem. Phys.* **92**, 508–517 (1990).
8. Y. Yang, S. Liang, B. Lu, J. Zhou, *Energy Environ. Sci.* **15**, 1192-1200 (2022).
9. Q. Chen, S. Chen, J. Ma, S. Ding, J. Zhang, *Nano Energy* **117**, 108897 (2023).
10. F. Yang, J. Long, J. A. Yuwono, H. Fei, Y. Fan, P. Li, J. Zou, J. Hao, S. Liu, G. Liang, Y. Lyu, X. Zheng, S. Zhao, K. Davey, Z. Guo, *Energy Environ. Sci.* **16**, 4630-4640 (2023).
11. W. Li, L. Huang, H. Zhang, Y. Wu, F. Wei, T. Zhang, J. Fu, C. Jing, J. Cheng, S. Liu, *Matter* **6**, 2312-2323 (2023).
12. S. Chen, Y. He, S. Ding, J. Zhang, *J. Phys. Chem. C* **127**, 7609-7617 (2023).
13. Y. Du, R. Kang, H. Jin, W. Zhou, W. Zhang, H. Wang, J. Qin, J. Wan, G. Chen, J. Zhang, *Adv. Funct. Mater.* **33**, 2304811 (2023).
14. S. Niu, B. Zhao, D. Liu, *ACS Appl. Mater. Interfaces* **15**, 25558-25566 (2023).
15. J. Sun, H. Ma, D. Wang, *J. Alloys Compd.* **947**, 169696 (2023).
16. F. Wei, T. Zhang, H. Xu, Y. Peng, H. Guo, Y. Wang, S. Guan, J. Fu, C. Jing, J. Cheng, S. Liu, *Adv. Funct. Mater.* **34**, 2310693 (2024).
17. Z. Zhang, W. Ling, N. Ma, J. Wang, X. Chen, J. Fan, M. Yu, Y. Huang, *Adv. Funct. Mater.* **34**, 2310294 (2024).
18. F. Wei, H. Xu, T. Zhang, W. Li, L. Huang, Y. Peng, H. Guo, Y. Wang, S. Guan, J. Fu, C. Jing, J. Cheng, S. Liu, *ACS Nano* **17**, 20643-20653 (2023).
19. S. Wang, Z. Huang, B. Tang, X. Li, X. Zhao, Z. Chen, C. Zhi, A. L. Rogach, *Adv. Energy Mater.* **13**, 2300922 (2023).
20. Y. Zhang, X. Zhang, X. Li, C. Chen, D. Yu, G. Zhao, *J. Alloys Compd.* **976**, 173041 (2024).
21. Y. Li, H. Jia, U. Ali, B. Liu, L. Li, L. Zhang, H. Wang, T. Wang, C. Wang, *Chem. Eng. J.* **483**, 149320 (2024).
22. J. Sun, Z. Wang, J. Zhang, D. Wang, *J. Energy Storage* **90**, 111716 (2024).
23. J. He, Y. Mu, B. Wu, F. Wu, R. Liao, H. Li, T. Zhao, L. Zeng, *Energy Environ. Sci.* **17**, 323-331 (2024).
24. J. Lee, W. Lee, S. Back, S. Y. Yi, S. Lee, S. Kim, J. Moon, D.-Y. Koh, K. Kim, S. Back, J. Lee, *EES Catalysis* **2**, 276-285 (2024).
25. J. Ma, A. Azizi, E. Zhang, H. Zhang, A. Pan, K. Lu, *Chem. Sci.* **15**, 4581-4589 (2024).
26. C. Guo, Y. Cao, Y. Gao, C. Zhi, Y. X. Wang, Y. Luo, X. J. Yang, X. Luo, *Adv. Funct. Mater.* **34**, 2314189 (2024).
27. J. L. Yang, H. H. Liu, X. X. Zhao, X. Y. Zhang, K. Y. Zhang, M. Y. Ma, Z. Y. Gu, J. M. Cao, X. L. Wu, *J. Am. Chem. Soc.* **146**, 6628-6637 (2024).
28. N. Li, Z. Yang, Y. Li, D. Yu, T. Pan, Y. Chen, W. Li, H. Xu, X. Guo, H. Pang, *Adv. Energy Mater.* 2024, DOI: 10.1002/aenm.202402846.

29. K. Wang, H. Li, Z. Xu, Y. Liu, M. Ge, H. Wang, H. Zhang, Y. Lu, J. Liu, Y. Zhang, Y. Tang, S. Chen, *Adv. Energy Mater.* **14**, 2304110 (2024).
30. Z. Chen, F. Wang, R. Ma, W. Jiao, D. Li, A. Du, Z. Yan, T. Yin, X. Yin, Q. Li, X. Zhang, N. Yang, Z. Zhou, Q.-H. Yang, C. Yang, *ACS Energy Lett.* **9**, 2858-2866 (2024).
31. X. Guo, H. Xu, Y. Tang, Z. Yang, F. Dou, W. Li, Q. Li, H. Pang, *Adv. Mater.* 2024, DOI: 10.1002/adma.202408317.
32. J. Hu, Z. Zhang, T. Deng, F. C. Cui, X. Shi, Y. Tian, G. Zhu, *Adv. Mater.* 36, e2401091 (2024).
33. Y. Zhao, Y. Wang, W. Xue, R. Cheng, X. Zheng, G. Zhu, D. Hu, H. Huang, C. Hu, D. Liu, *Adv. Mater.* **36**, e2403097 (2024).
34. Z. Li, W. Cao, T. Hu, Y. Hu, R. Zhang, H. Cui, F. Mo, C. Liu, C. Zhi, G. Liang, *Angew. Chem. Int. Ed. Engl.* **63**, e202317652 (2024).
35. W. Qu, J. Zhu, G. Cao, S. Chen, Y. Tan, B. Chen, M. Zhang, *Small* **20**, e2310475 (2024).
36. Y. Zhao, L. Zhang, Y. Zheng, H. Xu, Q. Jiang, T. Chen, K. S. Hui, K. N. Hui, L. Wang, C. Zha, *Small* 2024, DOI: 10.1002/smll.202402527.
37. Y. Lyu, J. A. Yuwono, P. Wang, Y. Wang, F. Yang, S. Liu, S. Zhang, B. Wang, K. Davey, J. Mao, Z. Guo, *Angew. Chem. Int. Ed. Engl.* **62**, e202303011 (2023).
38. Q. Chen, S. Chen, J. Zhang, *J. Power Sources* **556**, 232529 (2023).
39. W. Han, X. Li, *J. Power Sources* **580**, 233296 (2023).
40. H. X. Dang, A. J. Sellathurai, D. P. J. Barz, *Energy Storage Mater.* **55**, 680-690 (2023).
41. H. Xu, R. Zhang, D. Luo, J. Wang, K. Huang, J. Chi, H. Dou, X. Zhang, G. Sun, *Energy Storage Mater.* **63**, 103019 (2023).
42. W. Li, H. Xu, H. Zhang, F. Wei, T. Zhang, Y. Wu, L. Huang, J. Fu, C. Jing, J. Cheng, S. Liu, *Energy Environ. Sci.* **16**, 4502-4510 (2023).
43. Y. Ji, J. Xie, Z. Shen, Y. Liu, Z. Wen, L. Luo, G. Hong, *Adv. Funct. Mater.* **33**, 2210043 (2023).
44. G. Chen, Y. Kang, H. Yang, M. Zhang, J. Yang, Z. Lv, Q. Wu, P. Lin, Y. Yang, J. Zhao, *Adv. Funct. Mater.* **33**, 2300656 (2023).
45. H. Xu, R. Zhang, D. Luo, J. Wang, H. Dou, X. Zhang, G. Sun, *ACS Nano* **17**, 25291-25300 (2023).
46. G. Wang, Q. Yao, J. Dong, W. Ge, N. Wang, Z. Bai, J. Yang, S. Dou, *Adv. Energy Mater.* **14**, 2303221 (2023).
47. J. Wu, J. L. Yang, B. Zhang, H. J. Fan, *Adv. Energy Mater.* **14**, 2302738 (2023).
48. Z. Hu, X. Wang, W. Du, Z. Zhang, Y. Tang, M. Ye, Y. Zhang, X. Liu, Z. Wen, C. C. Li, *ACS Nano* **17**, 23207-23219 (2023).
49. P. Lin, G. Chen, Y. Kang, M. Zhang, J. Yang, Z. Lv, Y. Yang, J. Zhao, *ACS Nano* **17**, 15492-15503 (2023).
50. J. Hao, L. Yuan, Y. Zhu, X. Bai, C. Ye, Y. Jiao, S. Z. Qiao, *Angew. Chem. Int. Ed. Engl.* **62**, e202310284 (2023).
51. Y. Kang, G. Chen, H. Hua, M. Zhang, J. Yang, P. Lin, H. Yang, Z. Lv, Q. Wu, J. Zhao, Y. Yang, *Angew. Chem. Int. Ed. Engl.* **62**, e202300418 (2023).
52. N. Wang, Y. Ma, Y. Chang, L. Feng, H. Liu, B. Li, W. Li, Y. Liu, G. Han, *J. Colloid Interface Sci.* **665**, 491-499 (2024).
53. T. Huang, S. Wang, J. Wu, H. Hu, J. Wang, X. Zhang, Y. Gao, *J. Power Sources* **608**, 234658 (2024).

54. H. Yu, X. Cai, Z. Wang, Z. Yang, W. Liu, M. Ren, J. Yao, Q. Liu, C. Qiao, *Colloid Surface A* **684**, 133239 (2024).
55. W. Du, L. Miao, Z. Song, X. Zheng, C. Hu, Y. Lv, L. Gan, M. Liu, *Chem. Eng. J.* **484**, 149535 (2024).
56. W. Qu, C. Wen, B. Chen, Y. Cai, M. Zhang, *Sci. China Mater.* **67**, 2889–2897 (2024).
57. P. Jiang, Q. Du, C. Lei, C. Xu, T. Liu, X. He, X. Liang, *Chem. Sci.* **15**, 3357-3364 (2024).
58. Y. Xu, M. Zhang, R. Tang, S. Li, C. Sun, Z. Lv, W. Yang, Z. Wen, C. Li, X. Li, Y. Yang, *Energy Environ. Sci.* 2024, DOI: 10.1039/D4EE02592J.
59. W. Han, J. Zhao, X. Li, *Inorg. Chem. Front.* **11**, 5376-5383 (2024).
60. Q. Yue, Y. Wan, X. Li, Q. Zhao, T. Gao, G. Deng, B. Li, D. Xiao, *Chem. Sci.* **15**, 5711-5722 (2024).
61. X. Chen, Y. Zhao, Y. Zheng, H. Xu, Q. Jiang, T. Chen, K. S. Hui, K. N. Hui, L. Zhang, C. Zha, *J. Mater. Chem. A* **12**, 16892-16900 (2024).
62. W. Zong, J. Li, C. Zhang, Y. Dai, Y. Ouyang, L. Zhang, J. Li, W. Zhang, R. Chen, H. Dong, X. Gao, J. Zhu, I. P. Parkin, P. R. Shearing, F. Lai, K. Amine, T. Liu, G. He, *J. Am. Chem. Soc.* **146**, 21377-21388 (2024).
63. H. Wu, J. Hao, S. Zhang, Y. Jiang, Y. Zhu, J. Liu, K. Davey, S. Z. Qiao, *J. Am. Chem. Soc.* **146**, 16601–16608 (2024).
64. H. Liu, Z. Xu, B. Cao, Z. Xin, H. Lai, S. Gao, B. Xu, J. L. Yang, T. Xiao, B. Zhang, H. J. Fan, *Adv. Energy Mater.* **14**, 2400318 (2024).
65. K. K. Sonigara, J. V. Vaghasiya, M. Pumera, *Adv. Energy Mater.* 2024, DOI: 10.1002/aenm.202401321.
66. T. Su, W. Ren, M. Xu, P. Xu, J. Le, X. Ji, H. Dou, R. Sun, Z. Chen, *Adv. Energy Mater.* **5**, 2303221 (2024).
67. Y. Huang, Y. Wang, X. Peng, T. Lin, X. Huang, N. S. Alghamdi, M. Rana, P. Chen, C. Zhang, A. K. Whittaker, L. Wang, B. Luo, *Mater. Futur.* **33**, 035102 (2024).
68. Q. Liu, Z. Yu, K. Fan, H. Huang, B. Zhang, *ACS Nano* **18**, 22484-22494 (2024).
69. F. Li, C. Zhou, J. Zhang, Y. Gao, Q. Nan, J. Luo, Z. Xu, Z. Zhao, P. Rao, J. Li, Z. Kang, X. Shi, X. Tian, *Adv. Mater.* 2024, DOI: 10.1002/adma.202408213.
70. T. Liu, C. Lei, H. Wang, J. Li, P. Jiang, X. He, X. Liang, *Adv. Mater.* **36**, 2405473 (2024).
71. J. L. Yang, T. Xiao, T. Xiao, J. Li, Z. Yu, K. Liu, P. Yang, H. J. Fan, *Adv. Mater.* **36**, e2313610 (2024).
72. S. J. Zhang, J. Hao, H. Wu, Q. Chen, C. Ye, S. Z. Qiao, *Adv. Mater.* **36**, e2404011 (2024).
73. Q. Chen, J. Hao, Y. Zhu, S. J. Zhang, P. Zuo, X. Zhao, M. Jaroniec, S. Qiao, *Angew. Chem. Int. Ed. Engl.* 2024, DOI: 10.1002/anie.202413703.
74. T. Xiao, J. L. Yang, B. Zhang, J. Wu, J. Li, W. Mai, H. J. Fan, *Angew. Chem. Int. Ed. Engl.* **63**, e202318470 (2024).
75. H. Wang, X. Liu, J. Zhong, L. Du, S. Yun, X. Zhang, Y. Gao, L. Kang, *Small* **20**, e2306947 (2024).
76. S. Back, L. Xu, J. Moon, J. Kim, Y. Liu, S. Y. Yi, D. Choi, J. Lee, *Small* 2024, DOI: 10.1002/smll.202405487.